

## Accurate Liquid Water Path Retrieval from Low-Cost Microwave Radiometers Using Additional Information from a Lidar Ceilometer and Operational Forecast Models

NICOLAS GAUSSIAT, ROBIN J. HOGAN, AND ANTHONY J. ILLINGWORTH

*Department of Meteorology, University of Reading, Reading, United Kingdom*

(Manuscript received 11 September 2006, in final form 22 November 2006)

### ABSTRACT

Water clouds have an important impact on the radiative balance of the earth. The use of ground-based dual-frequency microwave radiometers to derive both liquid water path (LWP) and water vapor path (WVP) is well established, but uncertainties over the dry, water vapor, and liquid water absorption coefficients and the radiometric calibration can lead to errors in the retrieved LWP. A method in which additional information from a lidar ceilometer is used to identify the presence of liquid water clouds and their altitude is described. When such clouds are absent, the radiometric calibrations of the two frequencies are optimally adjusted so that the retrieved LWP is forced to zero; when they are present the calibrations are interpolated from the nearest clear-sky periods before and after, and the temperature of the cloud is used to refine the liquid water absorption coefficient (with the temperature profile taken from a forecast model). This procedure is insensitive to the choice of absorption model, removes the troublesome negative values of LWP that can be retrieved, and provides more accurate values of low LWP in thin clouds. Analysis shows that LWP as low as  $10 \text{ g m}^{-2}$  can be reliably retrieved, 90% of the time the error being less than 50%, and for LWP greater than  $20 \text{ g m}^{-2}$  the error is less than 10%. An additional advantage is that the retrieval can tolerate uncertainties in the various absorption coefficients and is unaffected by slow drifts in brightness temperature errors of up to 5 K. Previous techniques have required that these temperatures be accurate to 0.5 K or better, which entails careful calibration and can be quite difficult to achieve.

### 1. Introduction

Liquid water clouds have an important effect on the earth's energy balance (Slingo 1990; Hartmann et al. 1992), which is primarily determined by their liquid water path (LWP). For example, Marchand et al. (2003) show that a change in LWP of  $10 \text{ g m}^{-2}$  in a cloud with LWP of below  $50 \text{ g m}^{-2}$  alters the downwelling shortwave flux by about  $50 \text{ W m}^{-2}$ ; Hogan et al. (2004) found that in the midlatitudes about 20% of clouds between  $-10^\circ$  and  $-20^\circ\text{C}$  contain thin cloud layers of supercooled water with an LWP of about  $20 \text{ g m}^{-2}$ , but their presence in the liquid rather than the ice phase can lead to shortwave flux changes of about  $100 \text{ W m}^{-2}$ . Accurate observations of liquid water path are needed to evaluate the representation of liquid water clouds in global circulation models (GCMs) used for forecasting future climate and for numerical weather prediction (NWP). In most operational NWP models, production

of rain by collision and coalescence is parameterized by an autoconversion rate that depends upon the value of the cloud liquid water content in the model (e.g., Wilson and Ballard 1999). Over the oceans, microwave radiometry from a satellite has proven to be the most direct and accurate method of determining liquid water path (e.g., Greenwald et al. 1993), but this method fails over the land because of the variable emissivity of the surface. Weng et al. (1997) suggested that the minimum detectable LWP is about  $50 \text{ g m}^{-2}$ , and for values of  $200 \text{ g m}^{-2}$  the scatter of individual points between algorithms is about  $100 \text{ g m}^{-2}$ . Ground-based cloud observing stations such as those in the Atmospheric Radiation Measurement (ARM) Program or CloudNet (Illingworth et al. 2007, manuscript submitted to *Bull. Amer. Meteor. Soc.*, hereafter ILL) aim to sample the important climatic regimes and should be able to provide more accurate estimates of LWP than those achievable from a satellite.

Westwater et al. (2001) provide an excellent summary of how LWP can be derived from the brightness temperatures observed with ground-based dual-frequency microwave radiometers. The temperatures

---

Corresponding author address: Nicolas Gaussiat, Met Office, FitzRoy Road, Exeter, Devon, EX1 3PB, United Kingdom.  
E-mail: nicolas.gaussiat@metoffice.gov.uk

can be converted into two optical depths, each of which can then be expressed as a sum of three terms that depend upon the water vapor path (VWP), LWP, and the dry optical depth of the air column. The two equations can, in principle, be solved to yield values of VWP and LWP. The accuracies of the retrieved values of LWP and VWP depend upon the errors in the two observed brightness temperatures, the assumed mean radiating temperature and dry optical depth of the atmosphere, and the uncertainties in the mass absorption coefficient for water vapor and cloud liquid water at the two frequencies. For clouds with low LWP, uncertainties in these coefficients can lead to large errors in retrieved LWP and even to unphysical negative values of LWP.

In this paper we describe how independent lidar observations can be used to identify the presence and altitude of water clouds, which improves the retrieval in two ways. First, when liquid water clouds are absent, the LWP is set to zero so there are two independent equations linking the optical depths to VWP. An optimal estimation approach is used to derive two optical depth correction factors that are introduced into the two equations to account for uncertainties in the coefficients and errors in instrument calibration. If liquid water clouds are present, the value of the correction factor is obtained by interpolation of the values between the clear-sky periods before and after. The second way the lidar is used is in providing the altitude of the liquid clouds, which enables their temperature to be established using a forecast model temperature profile, and hence the integrated liquid absorption coefficient to be better defined. The procedure removes the troublesome negative values of LWP and provides accurate values of LWP for thin clouds. We applied this technique to the several years of data gathered in the CloudNet project (ILL), in which continuous radar, lidar, and radiometer observations were made over several years at three European observing sites; here we analyze observations made at Chilbolton, United Kingdom, and Palaiseau, France.

In section 2, we outline the standard technique for deriving LWP and VWP from the brightness temperatures and consider the accuracy obtained if the “statistical” or “climatological” mean values of the various coefficients are used in the retrieval, where the mean values are derived from one year’s operational NWP model data. In section 3, we analyze the improvement that can be achieved if the coefficients are computed from the atmospheric profile held in the model at each hour for a year, rather than using the mean value. Section 4 describes the further improvement obtained using the technique in which the LWP is forced to zero

when liquid clouds are absent and examines how robust this is to unknown variations in the coefficients. Then, in section 5, we discuss the accuracy of the technique and provide examples of retrievals of low values of LWP from supercooled clouds.

## 2. Background

### a. Theory of the retrieval technique

The “standard” technique to retrieve the LWP and VWP takes advantage of brightness temperature measurements at two frequencies, with one frequency in the water vapor absorption window and the other outside. The brightness temperature  $T_b$  measured by a vertically pointing ground-based microwave radiometer at a given frequency depends on the temperature and the absorption coefficients of the atmospheric components from the surface to the effective top of the atmosphere ( $H$ ) and can be written as

$$T_b = \int_0^H \alpha(z)T(z)\exp\left[-\int_0^z \alpha(z') dz'\right] dz + T_{\text{cos}}\exp(-\tau), \quad (1)$$

where  $T_{\text{cos}} \sim 2.73$  K is the cosmic background temperature,  $\tau = \int_0^H \alpha dz$  is the total optical depth, and  $\alpha$  is the atmospheric absorption coefficient due to oxygen, liquid water, and vapor at the microwave radiometer frequency. Introducing the mass absorption coefficients of the liquid water and vapor,  $\kappa_l$  and  $\kappa_v$ , and the dry absorption coefficient  $\alpha_d$ , values of  $\alpha$  are related to liquid water content (LWC) and vapor water content (VWC) by

$$\alpha = \kappa_l \text{LWC} + \kappa_v \text{VWC} + \alpha_d. \quad (2)$$

The relation between brightness temperature and absorption is nonlinear. The problem is simplified by introducing the mean radiating temperature:

$$T_{\text{mr}} = \frac{\int_0^H \alpha(z)T(z)\exp\left[-\int_0^z \alpha(z') dz'\right] dz}{\int_0^H \alpha(z)\exp\left[-\int_0^z \alpha(z') dz'\right] dz}. \quad (3)$$

In the standard technique, at a given frequency,  $T_{\text{mr}}$  can be estimated from radiosondes or an operational forecast model. Substituting (3) into (1) we have

$$T_b = T_{\text{mr}}[1 - \exp(-\tau)] + T_{\text{cos}}\exp(-\tau). \quad (4)$$

A first step to retrieve LWP and VWP is to convert the brightness temperatures into optical depths from (4):

$$\tau = \ln\left(\frac{T_{\text{mr}} - T_{\text{cos}}}{T_{\text{mr}} - T_b}\right). \quad (5)$$

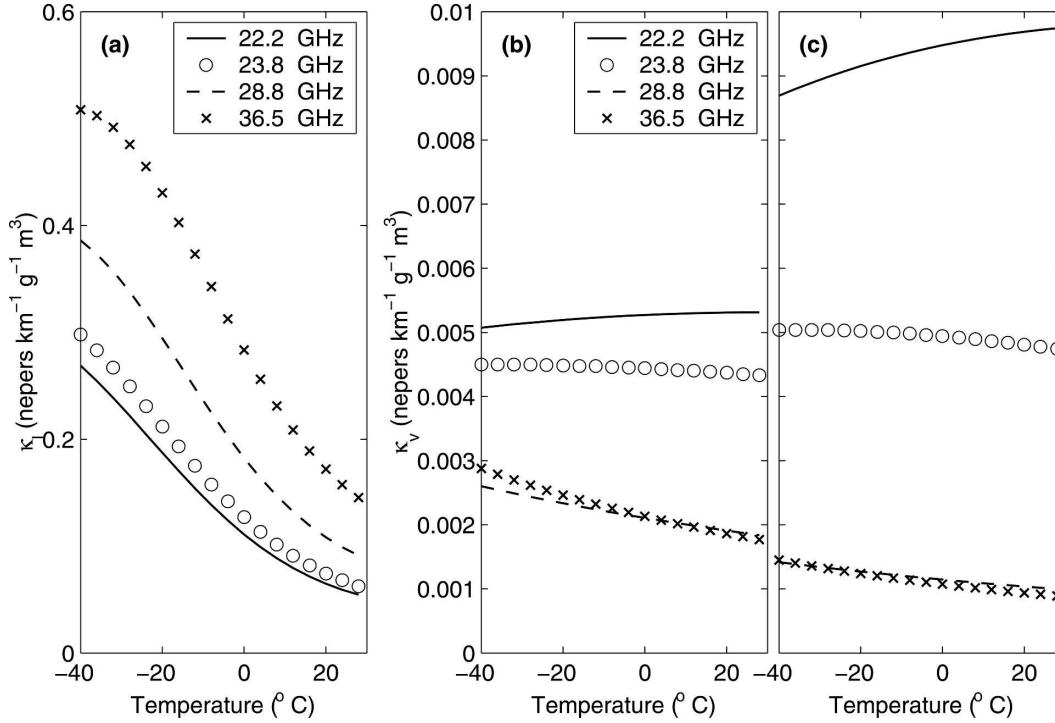


FIG. 1. (a) Variation of liquid water mass absorption coefficient  $\kappa_L$  with temperature; (b) variation of water vapor mass absorption coefficient  $\kappa_v$  with temperature at a pressure of 1000 hPa; (c) as in (b), but with a pressure of 500 hPa. Four commonly used frequencies are shown.

Then, considering the path-averaged values of the mass absorption coefficients,

$$k_l = \frac{1}{\text{LWP}} \int_0^H \kappa_l \text{LWC} dz, \quad k_v = \frac{1}{\text{VWP}} \int_0^H \kappa_v \text{VWC} dz, \quad (6)$$

the integration of (2) over the depth of the atmosphere gives at each frequency

$$\tau = k_l \text{LWP} + k_v \text{VWP} + \tau_d, \quad (7)$$

where  $\tau_d$  is the optical depth of the dry atmosphere. With two frequencies we have a pair of simultaneous equations of the form of (7), which we solve to obtain

$$\text{LWP} = \frac{k_{v2}\tau_1^* - k_{v1}\tau_2^*}{k_{l1}k_{v2} - k_{v1}k_{l2}}, \quad \text{VWP} = \frac{k_{l2}\tau_1^* - k_{l1}\tau_2^*}{k_{v1}k_{l2} - k_{l1}k_{v2}}, \quad (8)$$

where  $\tau^* = \tau - \tau_d$ , and the subscripts 1 and 2 represent the values at two frequencies.

### b. Natural variation of the coefficients

The mass absorption coefficient of liquid  $\kappa_l$  varies with temperature, while the mass absorption coefficient of vapor  $\kappa_v$  and the dry absorption coefficient  $\alpha_d$  vary with both temperature and pressure due to the broadening of the absorption lines. Figure 1 shows for various

frequencies the variations of  $\kappa_l$  and  $\kappa_v$  as a function of  $T$ . The vapor calculations were performed using the Liebe et al. (1993) absorption model. Comparisons with water vapor path derived during periods of clear skies from radiometers and the zenith wet delay from global positioning satellites by Keihm et al. (2002) suggest that the  $\kappa_v$  values are correct to better than 5%. For liquid water the Liebe et al. (1989) absorption model was employed; below 10°C values of  $\kappa_l$  from different models start to diverge (e.g., Westwater et al. 2001), with differences exceeding 10% for temperatures below 0°C when laboratory measurements of liquid water become difficult. As a result of the temperature and pressure dependence of the absorption coefficients, changes in the vertical profiles of temperature, pressure, vapor, and liquid produce variations of the coefficients  $k_l$ ,  $k_v$ , and  $\tau_d$  and the values of  $T_{\text{mr}}$ . To illustrate the natural variation of these coefficients, Fig. 2 shows time series of  $k_l$ ,  $k_v$ ,  $\tau_d$ ,  $T_{\text{mr}}$ , and  $\tau$  calculated at the two frequencies used at Chilbolton from 1 yr of Met Office mesoscale model hourly profiles of temperature, pressure, water vapor, and liquid water. Table 1 summarizes the climatological means and standard deviations of  $k_l$ ,  $k_v$ ,  $\tau_d$ , and  $T_{\text{mr}}$  calculated for the frequencies used at the Chilbolton and Palaiseau sites archived as part of the CloudNet project. These mean values and standard de-

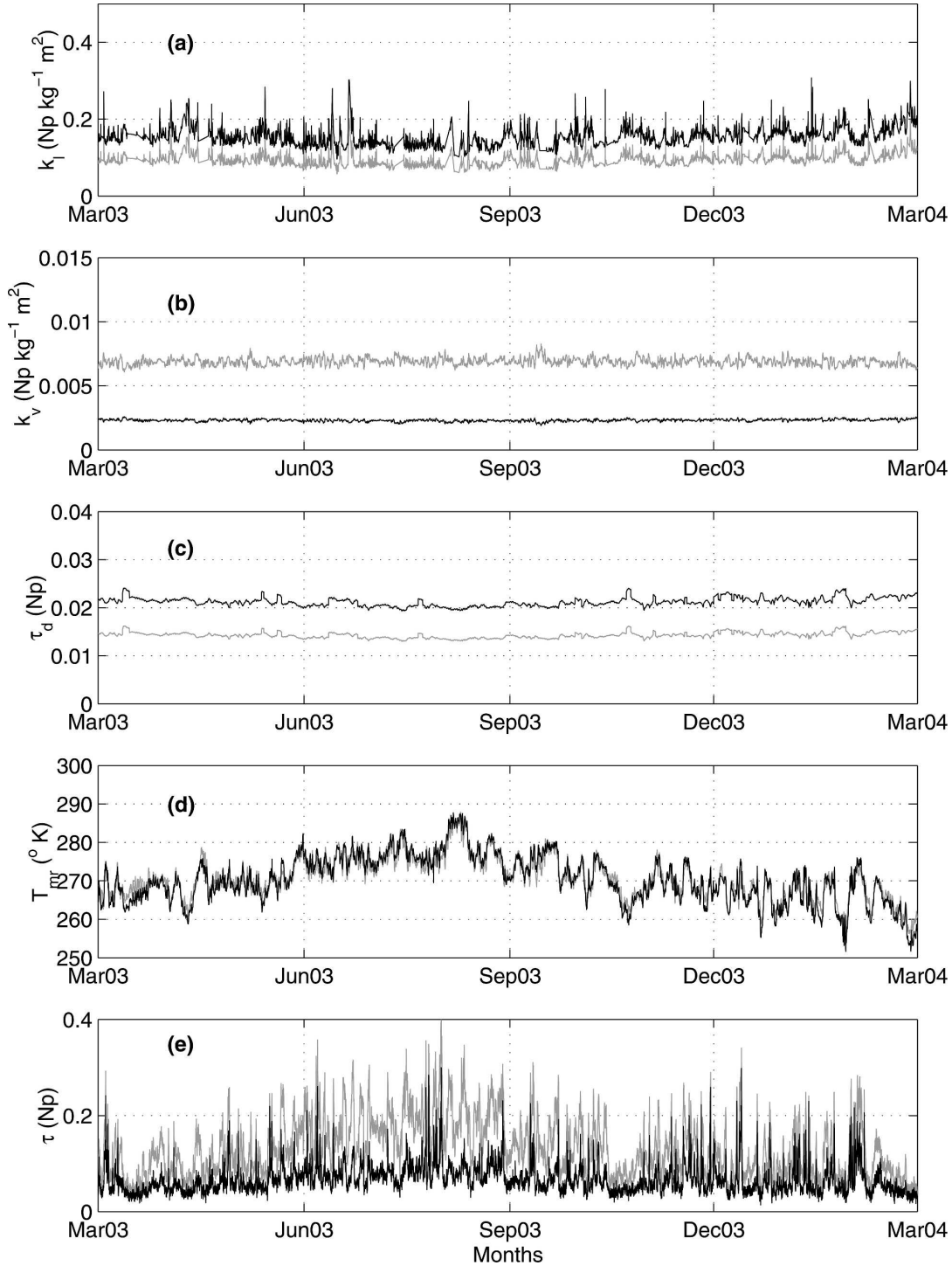


FIG. 2. One year of hourly values of the coefficients (a)  $k_l$ , (b)  $k_v$ , (c)  $\tau_d$ , (d)  $T_{mr}$ , and (e) the optical depth  $\tau$  calculated at 22.2 GHz (gray line) and 28.8 GHz (black line) from Met Office 0–5-h forecasts over Chilbolton. The mean optical depth and standard deviation at 22.2 GHz is  $0.133 \pm 0.059$  and at 28.8 GHz is  $0.067 \pm 0.030$ .

viations are consistent with those computed by Westwater et al. (2001) for 6 yr of arctic radiosonde soundings. Since the liquid water content is generally confined in a layer of negligible depth  $\Delta z$  compared to the

depth of the atmosphere, then  $k_l \sim \Delta z \kappa_l$ , where  $\kappa_l$  is taken at the mean temperature of the layer. Variations of  $k_l$  can be as large as 100% of the mean climatological value due to the sharp temperature dependence shown

TABLE 1. Climatological means and standard deviations of  $k_l$ ,  $k_v$ ,  $\tau_d$ , and  $T_{mr}$  calculated from 1 yr of Met Office 0–5-h forecasts for the frequencies used at Chilbolton and Palaiseau.

Site	Frequency	$\overline{k_L}$	$\Delta k_L$	$\overline{k_V}$	$\Delta k_V$	$\overline{\tau_D}$	$\Delta \tau_D$	$\overline{T_{mr}}$	$\Delta T_{mr}$
	(GHz)	(Np kg <sup>-1</sup> m <sup>2</sup> )		(10 <sup>-3</sup> Np kg <sup>-1</sup> m <sup>2</sup> )		(10 <sup>-3</sup> Np)		(°C)	
Chilbolton	22.2	0.094	±0.016	6.90	±0.29	14.27	±0.59	271	±5
	28.8	0.154	±0.024	2.31	±0.09	21.21	±0.88	270	±6
Palaiseau	23.8	0.109	±0.020	5.58	±0.06	15.32	±0.58	273	±6
	36.5	0.240	±0.039	2.16	±0.11	38.33	±1.48	269	±7

in Fig. 1a. Infrequent high values are associated with the occurrence of supercooled clouds. Since low-level clouds occur more often, the mean is found to be close to the minimum value, and the standard deviation is around 20% of the mean. It is clear that if a climatological average  $k_l$  were used in a retrieval, the LWP of supercooled clouds would typically be overestimated by a factor of 2. By contrast, the  $k_v$  variations appear small compared to  $k_l$ , the standard deviation of  $k_v$  being only 1%–5% of the mean.

### 3. Accuracy of retrieval algorithms using both fixed and variable coefficients

Variations of the coefficients  $k_l$ ,  $k_v$ ,  $\tau_d$ , and  $T_{mr}$  imply that a pair of measured brightness temperatures do not correspond to a single pair of LWP and VWP values. Therefore, when a mean state of the atmosphere above a given location is considered and the coefficients are fixed (e.g., using climatological values), LWP and VWP are retrieved with errors associated with the natural variability of the coefficients. To illustrate the problem, we have produced synthetic values of  $\tau$  and  $T_{mr}$  from 1 yr of 0–5-h model forecasts over Chilbolton and Palaiseau and converted them into synthetic brightness temperatures using (4). Then, we have used (8) with the mean values of the coefficients  $k_l$ ,  $k_v$ ,  $\tau_d$ , and  $T_{mr}$  from Table 1 to retrieve LWP and VWP values. Figure 3 shows the distributions of LWP errors for Chilbolton and Palaiseau obtained by taking the difference between the retrieved LWP and the ones produced directly from the model. Both distributions are skewed and exhibit large tails, with error values as large as 100 g m<sup>-2</sup>. Standard deviations of 26.6 g m<sup>-2</sup> at Chilbolton and 19.7 g m<sup>-2</sup> at Palaiseau indicate that the 23.8/36.5-GHz pair is preferable to 22.2/28.8 GHz for estimating LWP. Since the synthetic brightness temperatures are considered as perfect measurements, no measurement

errors have been introduced, so the standard deviations should be regarded as a lower limit on the retrieval error due purely to natural fluctuations in the coefficients.

Table 2 summarizes the optical depth uncertainties and consequent uncertainties in LWP for Chilbolton and Palaiseau arising from the use of fixed coefficients rather than the variable coefficients that correspond to the true state of the atmosphere. We use the standard deviations of the coefficients in Table 1 to compute the various contributions to the error in the total optical depth. Given a pair of LWP and VWP values, optical depth uncertainties  $\Delta\tau_l$  and  $\Delta\tau_v$  are related to the standard deviation of  $k_l$  and  $k_v$  by  $\Delta\tau_l = \Delta k_l \text{LWP}$  and  $\Delta\tau_v = \Delta k_v \text{VWP}$ . Since LWP and VWP vary, an estimate of the  $\tau_l$  and  $\tau_v$  uncertainties is obtained by considering the mean climatological values  $\overline{\text{LWP}}$  and  $\overline{\text{VWP}}$ . To calculate the uncertainties introduced by  $T_{mr}$  and  $T_b$  errors, since generally  $T_b = T_{mr}$ , from (5) we can approximate,  $\tau \sim (T_b - T_{\text{cos}})/T_{mr}$ , then an optical depth uncertainty  $\Delta\tau_{mr}$  is related to  $\Delta T_{mr}$  by  $\Delta\tau_{mr}/\tau = \Delta T_{mr}/T_{mr}$  and an optical depth uncertainty  $\Delta\tau_b$  is related to  $\Delta T_b$  by  $\Delta\tau_b = \Delta T_b/T_{mr}$ . Note that the fractional error in  $T_{mr}$  from Table 1 is about 2%, so the error  $\Delta T_{mr}$  is about 2% of the mean optical depth at each frequency. A brightness temperature error of 0.3 K is about 0.1% of the mean value of  $T_{mr}$ , so the value of  $\Delta\tau_b$  is about 0.001 for all frequencies. Then, assuming that the correlation between the coefficients is low (mainly because pressure and temperature variations are uncorrelated), we deduce that the total optical depth uncertainty is

$$\Delta\tau = \sqrt{\Delta\tau_l^2 + \Delta\tau_v^2 + \Delta\tau_d^2 + \Delta\tau_{mr}^2 + \Delta\tau_b^2}. \quad (9)$$

Using (8), we deduce that the retrieval errors  $\varepsilon_{\text{LWP}}$  and  $\varepsilon_{\text{VWP}}$  are related to the total optical depths calculated at two frequencies by

$$\varepsilon_{\text{LWP}} = \frac{\sqrt{(\overline{k_{v2}}\Delta\tau_1)^2 + (\overline{k_{v1}}\Delta\tau_2)^2}}{|\overline{k_{l1}}\overline{k_{v2}} - \overline{k_{v1}}\overline{k_{l2}}|}, \quad \varepsilon_{\text{VWP}} = \frac{\sqrt{(\overline{k_{l2}}\Delta\tau_1)^2 + (\overline{k_{l1}}\Delta\tau_2)^2}}{|\overline{k_{v1}}\overline{k_{v2}} - \overline{k_{v1}}\overline{k_{v2}}|}. \quad (10)$$

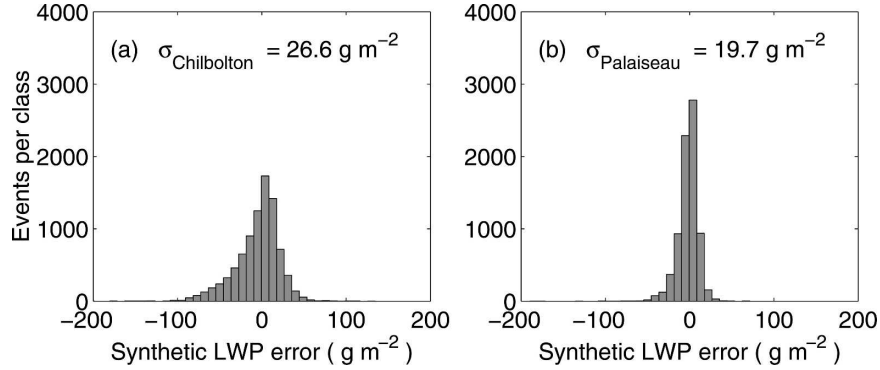


FIG. 3. Distributions of the differences between LWP values held in the NWP model and LWP values retrieved assuming constant coefficients and using perfect brightness temperatures calculated from the model data, for the frequency combination used at (a) Chilbolton and (b) Palaiseau.

Several values have been considered for  $T_b$  measurement accuracy. For perfect measurements ( $\Delta T_b = 0$ ), a remarkably good agreement is found between the estimated LWP errors (26.3 and 18.7  $\text{g m}^{-2}$ ) and the errors produced by the synthetic retrieval (26.6 and 19.7  $\text{g m}^{-2}$ ) with  $\sim 1\%$  difference for Chilbolton and  $\sim 5\%$  for Palaiseau. Westwater et al. (2001) used a 23.5/31.5-GHz pair and suggest that with careful attention given to the calibration of the radiometers, 0.3-K accuracy for the measured brightness temperature is achievable, and argue that the LWP error is  $\sim 25 \text{ g m}^{-2}$ . For the same measurement accuracy, our estimated errors are close, with 19.7  $\text{g m}^{-2}$  for Palaiseau and 28  $\text{g m}^{-2}$  for Chilbolton. As we can see from the breakdown of the optical depth uncertainties, the difference between the estimated errors arises from the water vapor optical depth uncertainty at 22.2 GHz that becomes larger close to the water vapor absorption line. When the brightness temperature accuracy is degraded to 1.5 K, as is common for unattended systems, errors in LWP are doubled.

In a “physical” retrieval the coefficients, rather than being held constant, are allowed to vary and are derived from temperature and humidity profiles from an operational forecast model or from independent obser-

vations, such as a radiosonde, or from the cloud height observed by radar or lidar. If the true value of these coefficients were known perfectly, then the errors for the various optical depths in Table 2 would be reduced to zero. However, the forecast model is not perfect, so we estimate the errors from the model by comparing the values of coefficients from the hourly model output with those from radiosondes and then calculate the values of  $\Delta\tau_l$ ,  $\Delta\tau_v$ ,  $\Delta\tau_d$ , and  $\Delta\tau_{mr}$  produced by such uncertainties.

First, we consider how the errors in  $k_l$  can be reduced by using a value derived from the temperature of the liquid layer detected by the lidar, rather than the constant climatological value from Table 1. The height is derived using the algorithm reported by Hogan et al. (2003). Figure 4a compares the values of  $k_l$  at 22 GHz derived from the 905-nm lidar ceilometer-derived cloud height and those from the height of the 94-GHz radar reflectivity-weighted profile, as proposed by Liljegren et al. (2001). Full specifications of the lidar and radar can be found in ILL. On many occasions the radar echo from the ice above the liquid water layer dominates the radar return, so that method overestimates the height, the temperature is too low, and the value of  $k_l$  is too high. Following Hogan et al. (2003),

TABLE 2. Optical depth uncertainties and LWP rms errors estimated in the case of a retrieval performed with fixed coefficients at 22.2/28.8 GHz (Chilbolton) and at 23.8/36.5 GHz (Palaiseau). Different values of brightness temperature measurement accuracy have been considered: respectively,  $\Delta T_b = 0, 0.3$ , and 1.5 K.

Site	Frequency (GHz)	$\Delta\tau_l$	$\Delta\tau_v$	$\Delta\tau_d$	$\Delta\tau_{mr}$ ( $\text{Np} \times 10^{-3}$ )	$\Delta\tau_b$	$\Delta\tau$	$\epsilon_{LWP}$ ( $\text{g m}^{-2}$ )
Chilbolton	22.2	0.85	4.69	0.59	2.60	0/1.11/5.36	5.46/5.57/7.78	26.3/28.0/54.5
	28.8	1.30	1.47	0.88	1.56	0/1.11/5.36	2.66/2.88/6.15	
Palaiseau	23.8	0.75	1.09	0.58	2.70	0/1.10/5.31	3.06/3.25/6.29	18.7/19.7/35.4
	36.5	1.45	1.83	1.48	2.17	0/1.11/5.38	3.52/3.69/6.58	

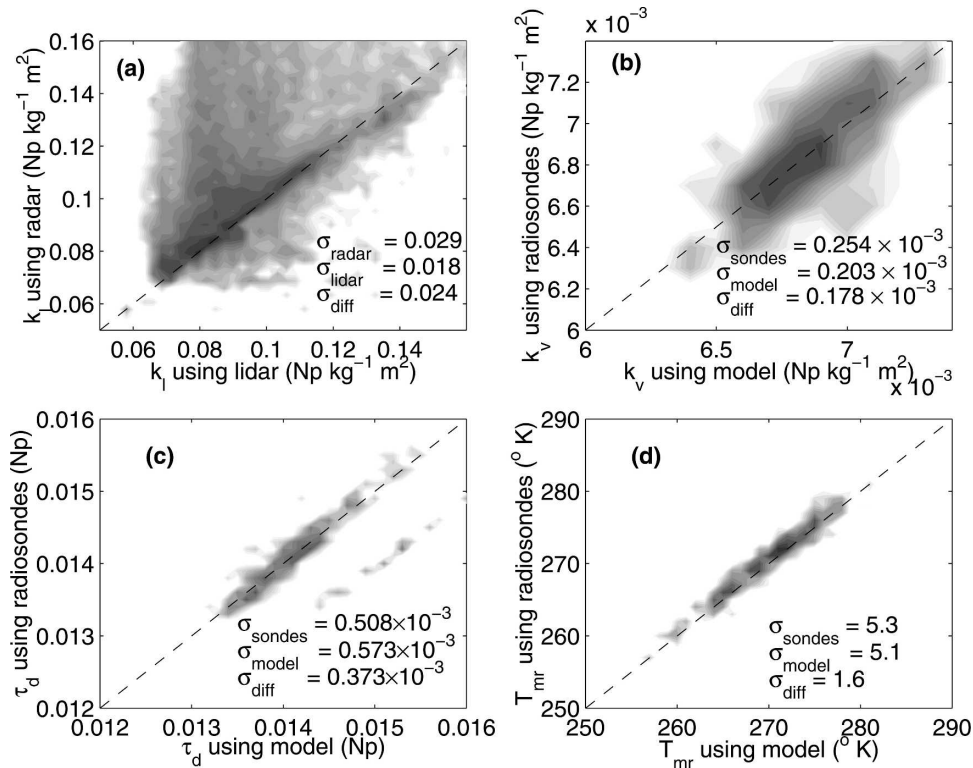


FIG. 4. (a) Value of  $k_l$  calculated at 22 GHz using temperature at lidar cloud-base height vs  $k_l$  calculated using the reflectivity-weighted mean cloud temperature. Values of (b)  $k_v$ , (c)  $\tau_d$ , and (d)  $T_{\text{mr}}$  are calculated at 22 GHz from 3 months (June, July, August) of Met Office 0–5-h forecasts vs values calculated using radiosonde measurements.

we estimate that most of the liquid layers are about 300 m deep, and their temperature should be known to 2°C. The slope of the 22.2-GHz  $\kappa_l$  curve in Fig. 1 suggests that an uncertainty of 2°C would introduce an error of  $0.006 \text{ Np kg}^{-1} \text{ m}^2$  in  $k_l$ . This is one-third of the error in the constant climatological value of  $k_l$  (0.016) in Table 1. Table 3 confirms that the use of a variable  $k_l$  reduces the error by about a factor of 3 for the four frequencies when compared to the error associated with the fixed coefficients in Table 2.

Next, in Fig. 4b, we compare the values of  $k_v$  from the model with those obtained from a sonde, the difference being a good estimate of how a specific hourly profile differs from that held in the model. Figure 4b shows that, whereas the spread of  $k_v$  around the climatological value is  $0.203 \text{ Np kg}^{-1} \text{ m}^2$ , the difference between the model and sonde has a standard deviation of only  $0.178 \text{ Np kg}^{-1} \text{ m}^2$  at 22.2 GHz. Table 3 shows that the resultant error  $\Delta\tau_v$  for the four frequencies is reduced by about 30% compared to the error using fixed values in Table 2. The same comparison for errors in  $\tau_d$  at 22.2 GHz is shown in Fig. 4c, where we see that using  $\tau_d$  from the model rather than using a constant climato-

logical coefficient reduces the standard deviation of  $\tau_d$  by about 40%. Comparing Table 3 with Table 2 confirms that the  $\Delta\tau_d$  error is reduced by about 40% at all frequencies when the retrieval with variable coefficients is used.

Finally, Fig. 4d shows that the difference in  $T_{\text{mr}}$  from the model and the sonde is about 1.6 K, whereas the standard deviation of  $T_{\text{mr}}$  from its climatological value was 5 K. Table 3 confirms that the standard deviation of  $\Delta\tau_{\text{mr}}$  for retrievals with variable coefficients is about one-third the value with the constant coefficients in Table 2. Westwater et al. (2001) analyzed 6 yr of sonde ascents in the arctic and reported a standard deviation of 6 K for  $T_{\text{mr}}$ , which also reduced by a factor of 3 when  $T_{\text{mr}}$  was calculated from the surface temperature. Finally, the error  $\Delta\tau_b$  depends only on the uncertainty in the measured  $T_b$  and is thus unaffected by the change from constant to variable coefficients and is identical in Tables 2 and 3.

The final column in Table 3 is the error in LWP produced from the total uncertainty in optical depth from the use of variable coefficients. Note that for such retrievals with errors of up to 0.3 K in observed  $T_b$ , the

TABLE 3. Same as in Table 2, but for a variable coefficients retrieval using lidar and operational model forecasts or radiosondes.

Site	Frequency	$\Delta\tau_l$	$\Delta\tau_v$	$\Delta\tau_d$	$\Delta\tau_{mr}$	$\Delta\tau_b$	$\Delta\tau$	$\epsilon_{LWP}$
	(GHz)	(Np $\times 10^{-3}$ )						(g m $^{-2}$ )
Chilbolton	22.2	0.34	2.91	0.37	0.79	0/1.11/5.54	3.06/3.25/6.33	12.9/16.1/49.5
	28.8	0.37	0.92	0.57	0.41	0/1.11/5.55	1.21/1.64/5.68	
Palaiseau	23.8	0.31	0.86	0.14	0.49	0/1.10/5.49	1.05/1.52/5.49	8.0/10.0/31.1
	36.5	0.38	1.37	0.50	0.34	0/1.11/5.57	1.54/1.90/5.78	

error in the retrieved LWP is dominated by the uncertainties in the model humidity profile. For the frequency pair 22.2 and 28.8 GHz the use of variable coefficients rather than constant ones reduces the error in LWP from 28.0 to 16.1 g m $^{-2}$ ; the equivalent figures for 23.8 and 36.5 GHz are from 19.7 to 10.0 g m $^{-2}$  and are consistent with the values of 25 and 10 g m $^{-2}$  (for a mean LWP of 106 g m $^{-2}$ ) obtained by Westwater et al. (2001) and the values of Liljegren et al. (2001). These figures assume that there is no error in  $k_l$  and  $k_v$ , associated with the absorption models and confirm that LWP should be more accurate for the 23.8/36.5-GHz pair. Once the  $T_b$  error reaches 1.5 K, then this  $T_b$  uncertainty dominates the error in the retrieved LWP.

Figure 5 shows histograms of LWP retrieved every 30 s using variable coefficients during  $\sim 400$  h of clear-sky conditions over Chilbolton and Palaiseau. After a bias of 20 g m $^{-2}$  at Palaiseau and 19.3 g m $^{-2}$  at Chilbolton (attributed to uncertainty in the absorption model) has been removed so that the mean LWP is zero, the standard deviation gives a measure of the retrieval error. This bias due to the choice of the absorption model is similar to the 10–25 g m $^{-2}$  reported by Zuidema et al. (2005) and the 15–30 g m $^{-2}$  deduced by Marchand et al. (2003). At Chilbolton, the distribution is broad and its lower part exhibits long tails that signal the occurrence of very large errors up to 200 g m $^{-2}$ . The error calculation suggests that a standard deviation of 50.7 g m $^{-2}$  should correspond to a brightness temperature uncertainty of 1.5 K. Such a poor accuracy suggests that, even if microwave radiometer channels were calibrated 3–4 times a month using a liquid nitrogen-cooled blackbody target, the drifts in the calibration were not corrected frequently enough. At Palaiseau an additional cross-calibration of the radiometer against another with a tipping capability was carried out. Westwater et al. (2001) have shown that this much more complex procedure can reduce errors in  $T_b$  to better than 0.3 K. However, Fig. 5 and the associated biases of 20 g m $^{-2}$  show that even with this more accurate  $T_b$ , errors still remain in the derivation of LWP.

#### 4. Optimal use of clear-sky periods to retrieve LWP

##### a. Principle

One of the goals of cloud-observing stations is to make use of the synergy between remote sensing instruments. Atmospheric profile information from radar or lidar can be transferred to radiometer retrieval algorithms to derive more accurate path-integrated liquid and vapor water contents, and these estimates can be used in turn to improve the quantitative profiling of the atmosphere along the line of sight of the collocated instruments. As a first step, retrievals with variable coefficients make use of temperature from a model forecast or radiosondes and cloud height from lidar or radar, but their benefit is generally jeopardized by radiometer calibration drifts, absorption model uncertainty, and hardware problems that are difficult to monitor when instruments are left unattended. A better retrieval takes advantage of the ability of lidar and radar to detect clear-sky conditions (or even ice-only conditions). In such conditions, LWP is theoretically zero, and both the calibration and the coefficients can be constrained. We define  $C$ , a calibration factor, as the difference between the measured optical depth  $\tau_m$  converted from the measured brightness temperature  $T_b$  using (5) and the theoretical optical depth calculated from LWP and VWP using a forward model. For a pair of measured optical depths at two different frequencies, using (7) we have

$$\tau_{m1} = k_{l1}LWP + k_{v1}VWP + \tau_{d1} + C_1, \quad (11)$$

$$\tau_{m2} = k_{l2}LWP + k_{v2}VWP + \tau_{d2} + C_2. \quad (12)$$

When a clear-sky situation is detected, LWP = 0, so by eliminating VWP between (11) and (12) we obtain

$$\frac{\tau_{m1} - \tau_{d1} - C_1}{k_{v1}} = \frac{\tau_{m2} - \tau_{d2} - C_2}{k_{v2}}. \quad (13)$$

Calibration factors  $C_1$  and  $C_2$  are now related to the optical depths measured at two frequencies, but there is an infinity of pairs ( $C_1$ ,  $C_2$ ) that satisfy (13). To constrain the problem further, the optimal estimation

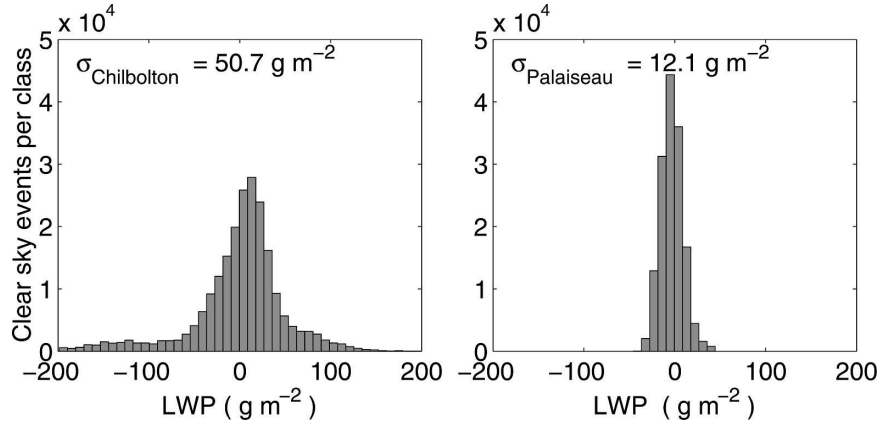


FIG. 5. Distributions and standard deviations of the retrieved LWP during clear-sky episodes during the years 2003–04 over Chilbolton and Palaiseau. Mean biases of  $20.0 \text{ g m}^{-2}$  at Palaiseau and  $19.3 \text{ g m}^{-2}$  at Chilbolton have been removed.

theory (Rodgers 2000) can be used to determine a best pair, assuming that errors are independent. Since radiometer receivers are physically separated, we assume that calibration drifts at different frequencies are uncorrelated. Coefficients are correlated, and therefore their errors are correlated. However, since the optimal method is expected to make a difference when calibration errors are bigger than retrieval errors, we consider that the calibration factors  $C_1$  and  $C_2$  are independent. The optimal pair of calibration coefficients minimizes the cost function:

$$J = \frac{1}{2} \left( \frac{C_1^2}{\sigma_1^2} + \frac{C_2^2}{\sigma_2^2} \right), \quad (14)$$

where  $\sigma_1$  and  $\sigma_2$  are the a priori rms errors of  $C_1$  and  $C_2$ . To find the minimum of the cost function with respect to  $C_1$  and  $C_2$ , we set  $\partial J / \partial C_1 = \partial J / \partial C_2 = 0$  to obtain

$$C_1 = - \frac{\sigma_1^2 \partial C_2}{\sigma_2^2 \partial C_1} C_2. \quad (15)$$

Considering (13), (15) becomes

$$C_1 = - \frac{k_{v2} \sigma_1^2}{k_{v1} \sigma_2^2} C_2. \quad (16)$$

Then, using (13) and (16) we deduce

$$C_1 = \frac{\tau_{m1} - \tau_{d1} - \frac{k_{v1}}{k_{v2}} (\tau_{m2} - \tau_{d2})}{1 + \left( \frac{k_{v1} \sigma_2}{k_{v2} \sigma_1} \right)^2}, \quad (17)$$

$$C_2 = \frac{\tau_{m2} - \tau_{d2} - \frac{k_{v2}}{k_{v1}} (\tau_{m1} - \tau_{d1})}{1 + \left( \frac{k_{v2} \sigma_1}{k_{v1} \sigma_2} \right)^2}. \quad (18)$$

It should be noted that  $\sigma_1$  and  $\sigma_2$  are included so that one may account for a known difference in the reliabil-

ity of the two frequencies. However, in the common situation that they are considered equally reliable, the equations can be simplified by setting  $\sigma_1 = \sigma_2 = 1$ . Values of  $C_1$  and  $C_2$  are calculated for all measurements in clear-sky periods, and, as it is more physically realistic to assume that the instrument calibration varies linearly in time than the LWP offset [as assumed by van Meijgaard and Crewell (2005)],  $C_1$  and  $C_2$  are linearly interpolated during cloudy periods.

Figure 6 demonstrates how the technique works for a day of data, 6 July 2004, at Palaiseau. Figure 6a shows profiles of lidar backscatter coefficient produced every 30 s. Weaker returns are generally due to aerosol or ice, while a backscatter exceeding  $2.5 \times 10^{-4} \text{ sr}^{-1} \text{ m}^{-1}$  and then falling by a factor of 20 in the 200 m above the peak value is identified as liquid water (Hogan et al. 2004). A measurement is flagged as a clear-sky event when no liquid water is identified. Since radiometers have a much larger field of view than the lidar, to avoid any false alarms, a succession of measurements are counted as clear-sky period when framed by 5 min of continuous clear-sky events. Several periods have been identified as clear sky using this technique and are shaded in gray in Figs. 6b and 6c. Figure 6b shows the time series of the correction coefficients at the two frequencies calculated using (17) and (18) during the identified clear-sky period and interpolated during the cloudy periods. The  $k_v$  and  $\tau_d$  coefficients have been computed at each frequency using the Met Office 0–5-h forecasts. In Fig. 6c the LWP produced by a retrieval using constant coefficients is compared to the LWP produced by the new technique that makes use of model and lidar information to constrain both coefficients and radiometer calibration. When the retrieval using constant coefficients is used a large bias, 25–50  $\text{g m}^{-2}$ , is visible from 0100 to 0400 UTC and from 0500 to

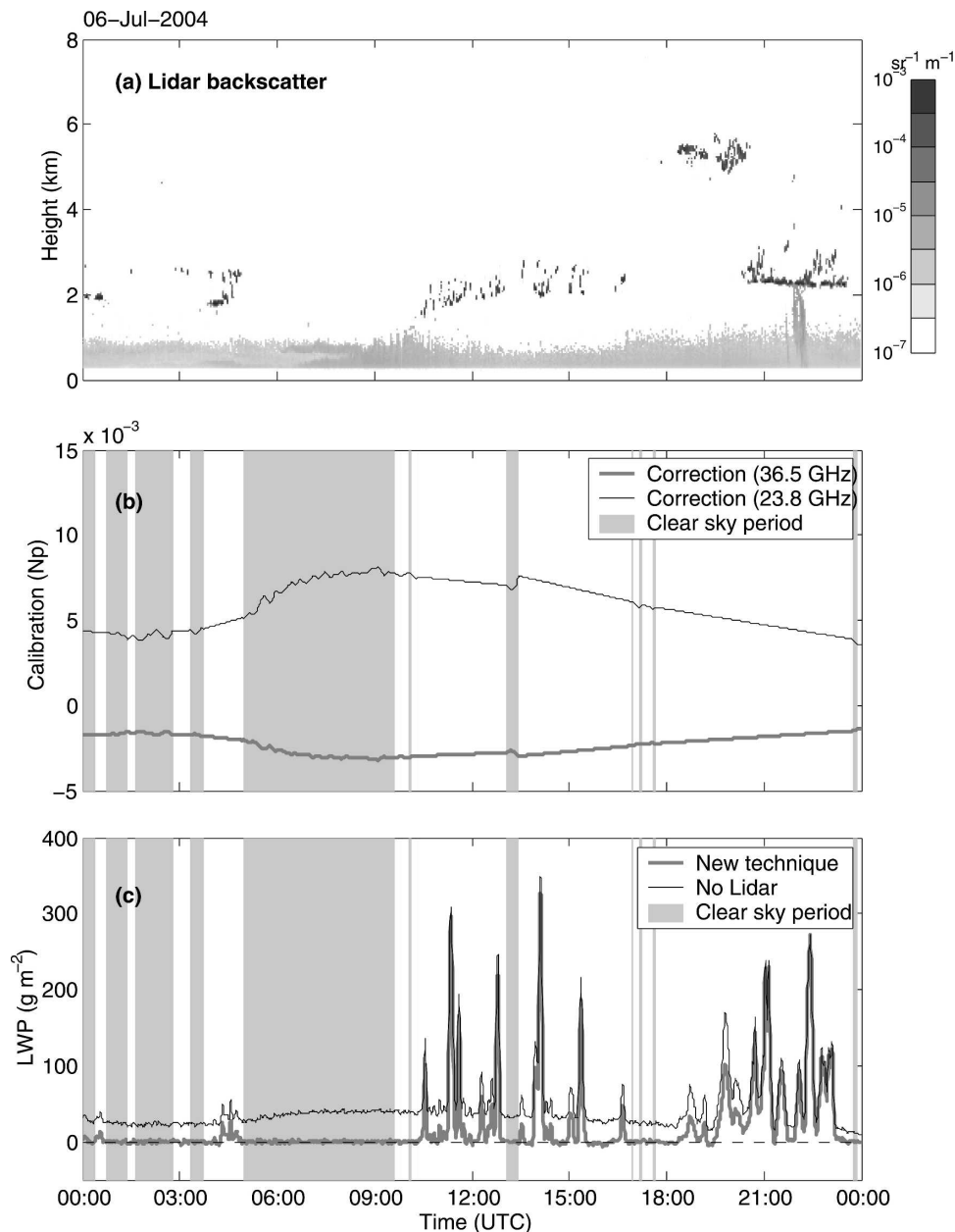


FIG. 6. (a) The 905-nm lidar backscatter coefficient at Palaiseau on 6 Jul 2004. (b) Identified clear-sky periods in gray and values of the correction coefficients deduced from these periods. (c) LWP retrieved using the new technique, compared to the retrieval using fixed coefficients.

1000 UTC in the clear-sky periods, and because this bias is varying, a mean bias correction would fail to solve the problem. When the optimal correction coefficients are used the bias is totally removed. Small LWP values in the range of 5–30  $\text{g m}^{-2}$  between 0400 and 0500 UTC that were smaller than the bias variations can now be retrieved with confidence. Since the correction coefficients are interpolated during the cloudy periods, nonzero values of LWP are also corrected, and

on many occasions we can see that the physical correction proposed here differs from a simple baseline subtraction (van Meijgaard and Crewell 2005).

*b. Robustness of the new method*

Methods that take advantage of cloud-free episodes to recalibrate microwave radiometers and constrain coefficients have been suggested before. Liljegren (2000) proposed an automatic recalibration technique for the

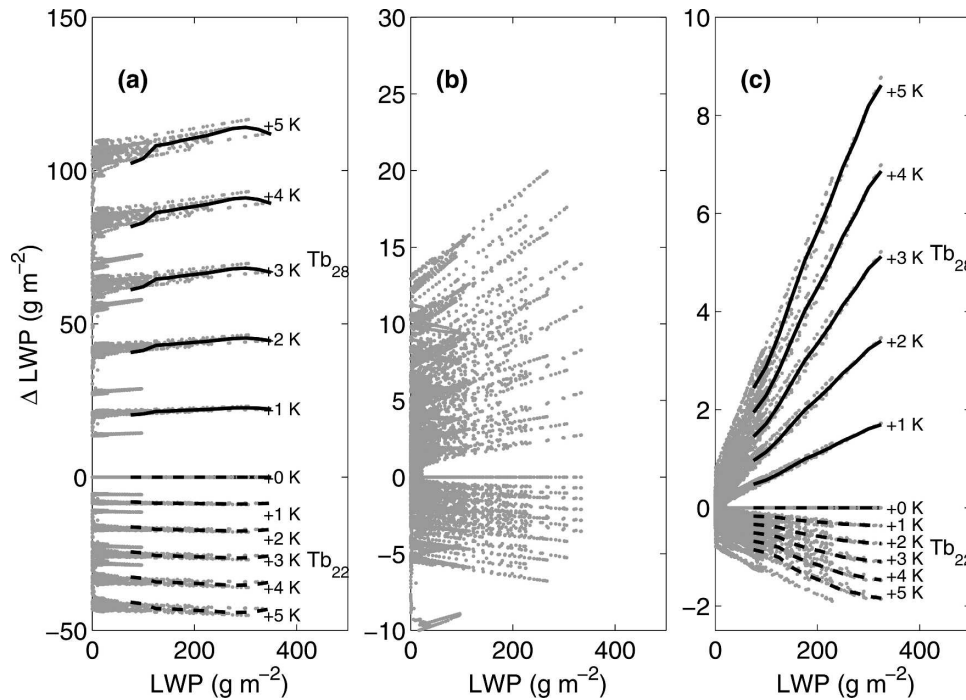


FIG. 7. Retrieved LWP errors as a function of the LWP when offsets ranging from 1 to 5 K are applied to one of the brightness temperatures: (a) constant coefficients, (b) subtraction of clear-sky LWP (van Meijgaard and Crewell 2005), and (c) retrieval with optimal use of clear-sky periods.

radiometers of the ARM Program that involves running a fast tip-curving calibration each time a clear-sky period is detected, and van Meijgaard and Crewell (2005) used a postprocessing technique that computes a local offset correction from the clear-sky LWP values within a  $\pm 5$  h Gaussian running window. To demonstrate the robustness of our new postprocessing technique, we have tested the sensitivity of the retrieved LWP to constant offsets applied to each of the measured brightness temperatures ( $T_b$ s) for a month of retrieved LWP at Chilbolton. Figure 7 presents, for different retrieval methods, the errors produced by offsets ranging from 1 to 5 K applied to the brightness temperature at 22 and 28 GHz. Figure 7a shows the LWP error obtained when using constant coefficients in the retrieval. A bias applied on one of the brightness temperatures results in an error in the retrieved LWP. The error dependence with LWP is small, so we can approximate the error with brightness temperature as  $\sim -8 \text{ g m}^{-2} \text{ K}^{-1}$  at 22 GHz and  $\sim 20 \text{ g m}^{-2} \text{ K}^{-1}$  at 28 GHz. These values are consistent with those of Crewell and Lohnert (2003). Bias values of up to  $100 \text{ g m}^{-2}$  occur for a 5-K brightness temperature bias at 28 GHz. Figure 7b shows the error when an LWP offset subtraction correction using a  $\pm 5$  h Gaussian weighted window is applied (van Meijgaard and Crewell 2005). The dependence with LWP remains, but improvement is sub-

stantial since the spread of the biases is reduced by a factor of  $\sim 10$ . Figure 7c shows the LWP error when the new technique is used. At  $\text{LWP} = 0$ , the error is reduced to  $1 \text{ g m}^{-2}$  and increases linearly with LWP and scales with the value of brightness temperature bias. Expressed in relative terms, the LWP error is  $\sim 0.1\% \text{ K}^{-1}$  when the bias is applied at 22 GHz and  $\sim 0.5\% \text{ K}^{-1}$  at 28 GHz. By making an optimal use of the clear-sky events, the new technique succeeds well beyond other techniques in removing the effect of a constant bias on one of the brightness temperatures.

### c. Accuracy of the new method

During cloudy periods, calibration factors are interpolated linearly, but drifts may not vary linearly, so the accuracy of the retrieved LWP depends on the time to the nearest clear-sky period. To get an estimate of the accuracy of the new technique, we considered changes in the calibration factors,  $\Delta C_1$  and  $\Delta C_2$ , from the beginning to the end of the cloudy period. We used several months of retrieved  $C_{22}$  and  $C_{28}$  at Chilbolton in order to get a good sample of all possible calibration changes over different lengths of cloudy periods. Figures 8a and 8b show, respectively, PDFs of  $\Delta C_{22}$  and  $\Delta C_{28}$ . As expected, at both frequencies, the distribution of the changes becomes broader and the median value of the changes increases with the length of cloudy pe-

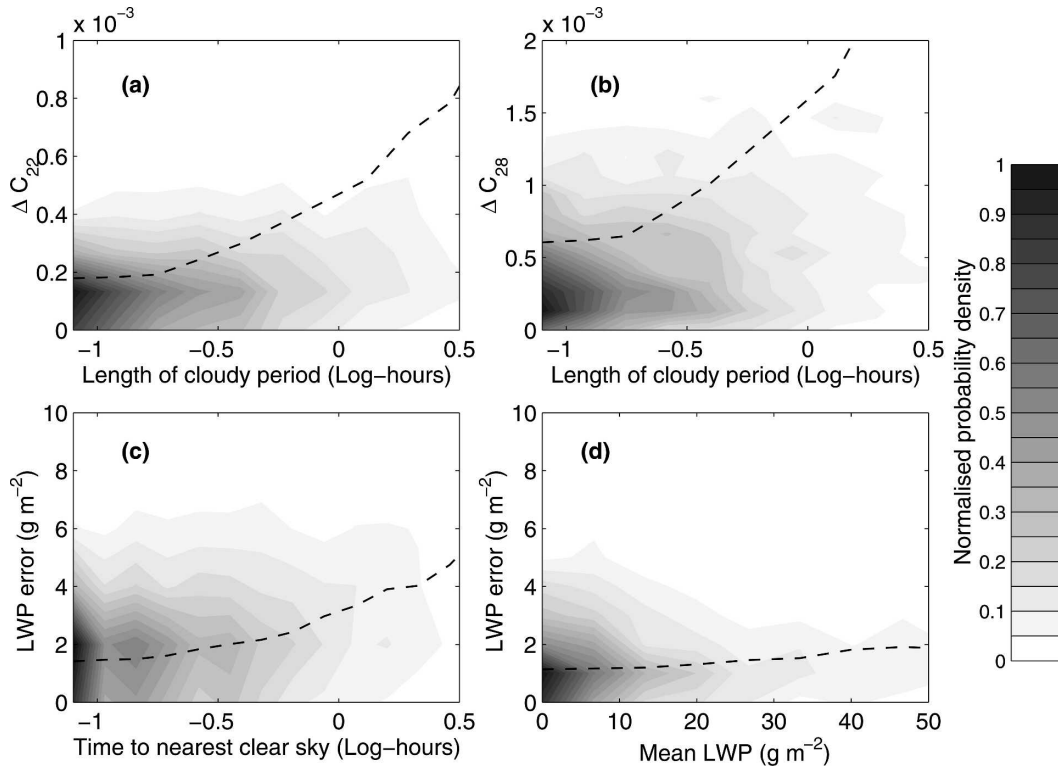


FIG. 8. PDF and median of calibration changes at (a) 22 and (b) 28 GHz as a function of the length of the cloudy period, calculated from Chilbolton radiometers and lidar measurements using the new method. (c) PDF and median of the LWP error as a function of the time to the nearest clear sky. (d) PDF and median of the LWP error as a function of the mean LWP.

riod. By replacing  $\Delta\tau_1$  and  $\Delta\tau_2$  in (10) by  $\Delta C_1$  and  $\Delta C_2$  (here  $\Delta C_{22}$  and  $\Delta C_{28}$ ), the PDFs of the changes in calibration can be used to get an estimate of the LWP error as a function of the time to the nearest clear-sky period. The PDF of the error is presented in Fig. 8c. Overall, 90% of the time the error is less than  $7 \text{ g m}^{-2}$ . The median of the error increases with the time to the nearest clear-sky event. It is found to be around  $1.5 \text{ g m}^{-2}$  (which corresponds to the minimum sensitivity of the radiometers) for measurements made 5 min after a clear-sky event, and increases to  $3.5 \text{ g m}^{-2}$  when the closest clear sky is 1 h away. As, on average, deeper systems tend to have larger horizontal extensions and higher mean LWP, using the same dataset, we also produced a PDF of the LWP error as a function of the mean LWP over the cloudy period. The result is presented Fig. 8d. The PDF of the error suggests that for 90% of the measurements made in cloudy periods the error is less than  $5 \text{ g m}^{-2}$ , which is better than any other retrieval. The median of the error increases from 1 to  $2 \text{ g m}^{-2}$  when the mean LWP increases from 0 to  $50 \text{ g m}^{-2}$ . In summary, the retrieval error is better than 10% for 90% of the measured LWPs greater than  $30 \text{ g m}^{-2}$ , for 70% of the measured LWPs greater than  $20 \text{ g m}^{-2}$ ,

and 50% of all the measurements. With such high accuracy, the new technique is particularly adapted to mixed-phase clouds in which LWP is often too small to be determined by less accurate retrievals. Figure 9 presents a case of altocumulus with embedded supercooled layers. Figure 9a shows the radar reflectivity observed on 2 August 2004 at Chilbolton. In Fig. 9b, the lidar identifies strong returns due to supercooled layers at three levels around 3, 5, and 7 km. The optimal use of clear-sky and ice-only periods allows us to estimate LWP in this layer with an accuracy of  $5 \text{ g m}^{-2}$ . This particular case also demonstrates the superiority of the lidar, rather than radar, to estimate liquid layer height and correctly derive the  $k_l$  coefficient. At around 1400 UTC, the reflectivity is dominated by insects present in the boundary layer, and the height of the liquid layer is set too low compared to the correct height of the clouds detected by the lidar.

### 5. Conclusions

A new technique has been developed that uses additional information from model forecasts and lidar observations to improve the accuracy of the LWP re-

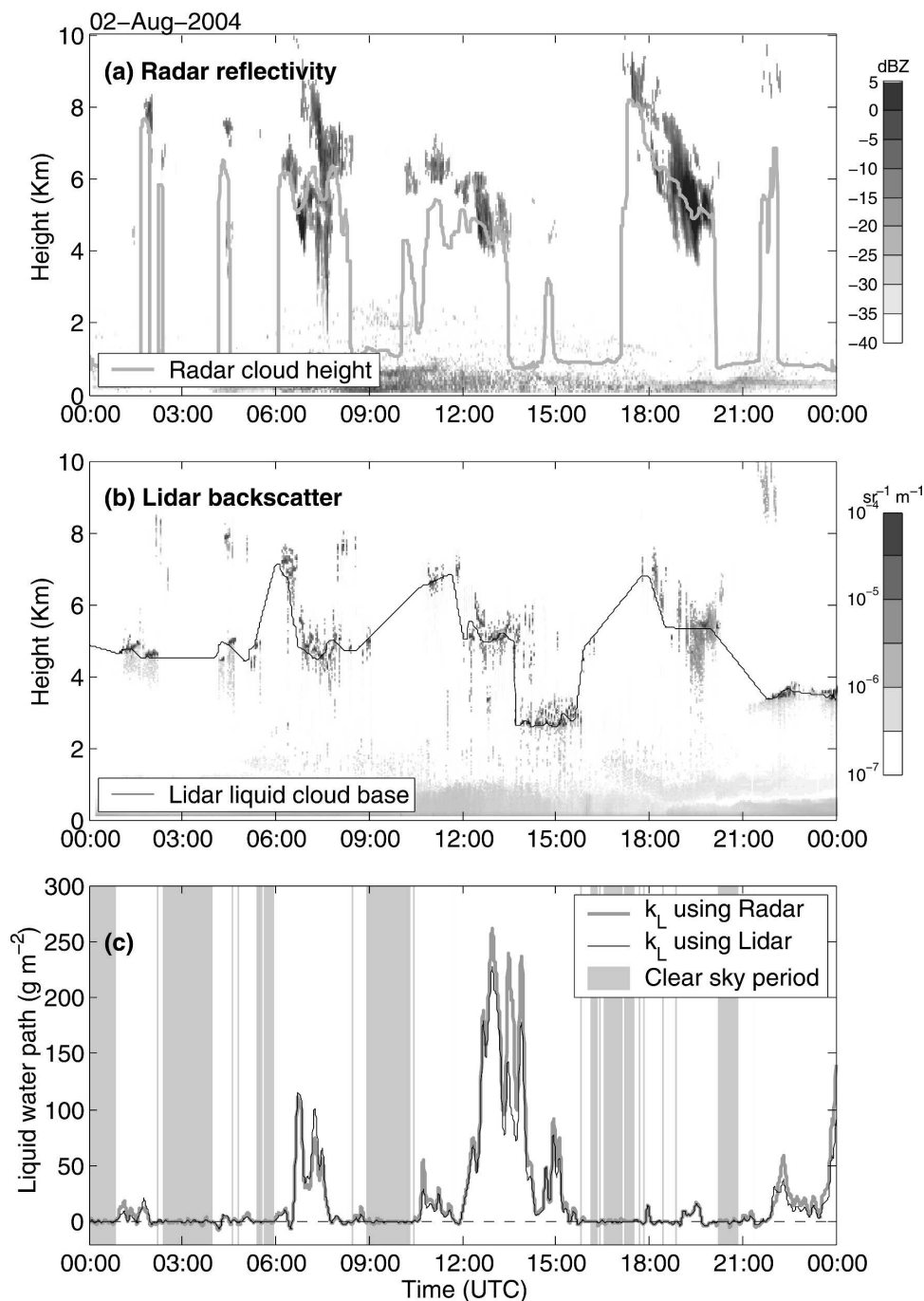


FIG. 9. Observations of supercooled layers on 2 Aug 2004: (a) radar reflectivity and mean target height; (b) lidar backscatter coefficient and lidar cloud height; (c) retrieved LWP with optimal use of clear-sky periods, with  $k_l$  calculated from model temperature and radar cloud height (in gray) and lidar cloud height (in black).

trieved from microwave radiometers. First, we have shown that the pressure, temperature, and humidity fields obtained from the model 0–5-h forecast combined with lidar cloud height observations can be used to predict the coefficients, which reduces the rms error

in LWP from 25–30  $\text{g m}^{-2}$  (from fixed coefficients) to 10–15  $\text{g m}^{-2}$ , assuming that the calibration of the radiometers is well behaved, with brightness temperatures accurate to 0.3 K. As has been recognized, the maintenance of such accuracy is not easy and increases the

cost of radiometer systems substantially. The original aspect of the technique presented in this paper is the continuous optimal correction of the radiometer calibration using clear-sky or ice-only periods detected by the lidar, when the LWP should be zero. We have tested the robustness of the new technique by applying large biases (up to 5 K) to the brightness temperatures and shown that the error introduced to the LWP is only  $0.5\% \text{ K}^{-1}$ . Using time series of corrections applied to the calibration, we have shown that the error on the retrieved LWP increases with time to the nearest clear-sky event, but in 90% of the observations the error is small and remains under  $5 \text{ g m}^{-2}$ . An optimal processing of lidar observations to detect clear-sky and ice-only conditions is necessary to ensure the quality of the retrieved LWP. Ice-only conditions are not always straightforward to detect, and false alarms that occur when liquid above thick ice is not seen by the lidar can occasionally affect the quality of the retrieval. Overall, considering the large positive impact, we recommend the use of the new technique for the development of future observing cloud stations fitted with low-cost radiometers and a lidar ceilometer that can be left unmanned without compromising the high quality of the retrieved LWP.

*Acknowledgments.* We acknowledge the CloudNet project (European Union Contract EVK2-2000-00611) for providing the Met Office mesoscale model data, which were produced by the Met Office and the University of Reading. CloudNet also provided the Instrument Synergy/Target Categorization data, which were produced by the University of Reading using measurements from the Chilbolton Facility for Atmospheric and Radio Research, part of the Rutherford Appleton Laboratory, and from SIRTA, operated by the Institut Pierre Simon Laplace (IPSL). This research also benefited from NERC Grant NE/D005205/1

## REFERENCES

- Crewell S., and U. Löhnert, 2003: Accuracy of cloud liquid water path from ground-based microwave radiometry 2. Sensor accuracy and synergy. *Radio Sci.*, **38**, 8042, doi:10.1029/2002RS002634.
- Greenwald, T. J., G. L. Stephens, T. H. Vonder Haar, and D. L. Jackson, 1993: A physical retrieval of cloud liquid water over the global oceans using Special Sensor Microwave/Imager (SSM/I) observations. *J. Geophys. Res.*, **98**, 18 471–18 488.
- Hartmann, D. L., M. E. Ockert-Bell, and M. L. Michelsen, 1992: The effect of cloud type on Earth's energy balance: Global analysis. *J. Climate*, **5**, 1281–1304.
- Hogan, R. J., P. N. Francis, H. Flentje, A. J. Illingworth, M. Quante, and J. Pelon, 2003: Characteristics of mixed-phase clouds. Part I: Lidar, radar and aircraft observations from CLARE'98. *Quart. J. Roy. Meteor. Soc.*, **129**, 2089–2116.
- , M. D. Behera, E. J. O'Connor, and A. J. Illingworth, 2004: Estimate of the global distribution of stratiform supercooled liquid water clouds using the LITE lidar. *Geophys. Res. Lett.*, **31**, L05106, doi:10.1029/2003GL018977.
- Illingworth, A. J., and Coauthors, 2007: Cloudnet: Continuous evaluation of cloud profiles in seven operational models using ground-based observations. *Bull. Amer. Meteor. Soc.*, **88**, 883–898.
- Keihm, S. J., Y. Bar-Sever, and J. C. Liljegren, 2002: WVR-GPS comparison measurements and calibration of the 20–32 GHz tropospheric water vapor absorption model. *IEEE Trans. Geosci. Remote Sens.*, **40**, 1199–1210.
- Liebe, H. J., T. Manabe, and G. A. Hufford, 1989: Millimeter-wave attenuation and delay rates due to fog/cloud conditions. *IEEE Trans. Antennas Propag.*, **37**, 1617–1623.
- , G. A. Hufford, and M. G. Cotton, 1993: Propagation modelling of moist air and suspended water/ice particles at frequencies below 1000GHz. *Proc. AGARD 52d Specialists' Meeting of the Electromagnetic Wave Propagation Panel*, Palma de Mallorca, Spain, AGARD, 3.1–3.10.
- Liljegren, J. C., 2000: Automatic self-calibration of ARM microwave radiometers. *Microwave Radiometry and Remote Sensing of the Earth's Surface and Atmosphere*, P. Pampaloni and S. Paloscia, Eds., VSP Press, 433–443.
- , E. E. Clothiaux, G. Mace, S. Kato, and X. Dong, 2001: A new retrieval for cloud liquid water path using a ground-based microwave radiometer and measurements of cloud temperature. *J. Geophys. Res.*, **106**, 14 485–14 500.
- Marchand, R., T. P. Ackerman, E. R. Westwater, S. A. Clough, K. Cady-Pereira, and J. C. Liljegren, 2003: An assessment of microwave absorption models and retrieval of cloud liquid water using clear-sky data. *J. Geophys. Res.*, **108**, 4773, doi:10.1029/2003JD003843.
- Rodgers, C. D., 2000: *Inverse Methods for Atmospheric Sounding: Theory and Practice*. World Scientific, 238 pp.
- Slingo, A., 1990: Sensitivity of the earth's radiation budget to changes in low clouds. *Nature*, **343**, 49–51.
- van Meijgaard, E., and S. Crewell, 2005: Comparison of model predicted liquid water path with ground-based measurements during CLIWA-NET. *Atmos. Res.*, **75**, 201–226.
- Weng, F., N. C. Grody, R. Ferrar, A. Basist, and D. Forsyth, 1997: Cloud liquid water climatology from the special sensor microwave/imager. *J. Climate*, **10**, 1086–1098.
- Westwater, E. R., Y. Han, M. D. Shupe, and S. Y. Matrosov, 2001: Analysis of integrated cloud liquid and precipitable water vapor retrievals from microwave radiometers during the Surface Heat Budget of the Arctic Ocean project. *J. Geophys. Res.*, **106**, 32 019–32 030.
- Wilson, D. R., and S. P. Ballard, 1999: A microphysically based precipitation scheme for the UK Meteorological Office Unified Model. *Quart. J. Roy. Meteor. Soc.*, **125**, 1607–1636.
- Zuidema, P., E. R. Westwater, C. Fairall, and D. Hazen, 2005: Ship-based liquid water path estimates in marine stratocumulus. *J. Geophys. Res.*, **110**, D20206, doi:10.1029/2005JD005833.